CHALMERS

UNIVERSITY OF TECHNOLOGY

Acceleration-based wheel slip control realized with decentralised electric drivetrain systems

N.B. When citing this work, cite the original published paper.

(article starts on next page)

IET Electrical Systems in Transportation

ORIGINAL RESEARCH

The Institution of Engineering and Technology WILEY

Acceleration-based wheel slip control realized with decentralised electric drivetrain systems

Bowen Jiang ⓘ | Nimananda Sharma | Yujing Liu | Chuan Li

Department of Electrical Engineering, Chalmers University of Technology, Gothenburg, Sweden

Correspondence

Bowen Jiang, Department of Electrical Engineering, Chalmers University of Technology, Hörsalsvägen 11A, Gothenburg, Sweden.
Email: bowen.jiang@chalmers.se

Abstract

Traction control is one of the most important functions in vehicle drivetrain systems. When a vehicle is driven on a low-friction road surface, loss of traction force can cause the driven wheels to spin. This reduces vehicle acceleration performance and can even cause the driver to lose control of the vehicle. The high bandwidth of electric machine control in electric vehicles gives more possibilities to regulate driving torque on wheels and prevent wheel spin. An acceleration-based wheel slip control is designed and investigated. Compared to traditional slip-based traction control, the proposed method does not depend on the estimation of the vehicle speed and only relies on the driven wheel rotational acceleration. The control method is verified using the simulation of an electric vehicle with a decentralised electric drivetrain system. The vehicle and the electric drive are modelled in CarMaker and PLECS, respectively. The simulation results show that the proposed method is able to prevent the driven wheel from spinning when the vehicle is accelerated on an ice road. In addition, the control is fast enough and requires only half a second to reduce the wheel acceleration to a normal range.

KEYWORDS

decentralised electric drivetrain systems (DEDSs), electric vehicles (EVs), traction control systems (TCSs), wheel slip control

1 | INTRODUCTION

With the fast development of transportation electrification, more and more new technologies based on electric vehicles are emerging. Decentralised electric drivetrain systems (DEDSs) are described as drivetrain systems having multiple electric machines as torque/power sources [1]. For example, it is possible to use two electric machines to drive two rear wheels independently or use four electric machines to drive all four wheels independently. DEDSs show advantages in many different aspects. Firstly, they normally have more compact structures that are very helpful in improving the flexibilities of drivetrain layouts and realise modular design [2, 3]. Secondly, higher transmission efficiency can be achieved due to shorter drivetrains and optimal torque distributions [4, 5]. Thirdly, DEDSs can make more complex vehicle control strategies appliable and enhance vehicle dynamic performance, such as steering manoeuvrability [3, 6] and slip ratio control [7].

The slip ratio is used to describe the difference between the driven wheel linear speed and the vehicle speed [8]. When a vehicle is driven on a low friction surface, such as an ice road, the driven wheels may spin during acceleration. During the spinning of the driven wheels, the traction force given by the road surface to the tire surface already reaches its limit and starts to drop. As a result, the excess driving torque from the vehicle drivetrain system only accelerates the rotational mass, such as driven wheels and transmission gears. Therefore, the acceleration performance of the vehicle will be reduced. In this case, the slip ratios of driven wheels will also largely increase [9]. Traction control systems (TCSs) are used to control the slip ratios within a correct range and avoid spinning [10].

In conventional internal combustion vehicles, the TCSs can be realised by applying braking force to the wheels that are spinning [11]. However, the response speeds can be limited due to the control of hydraulic systems [12]. In electric vehicles, due to the high bandwidth of electric machine controllers, the

torque applied on driven wheels can be controlled more precisely and with high dynamic performance [13]. Therefore, driven wheels can be prevented from spinning by reducing the torque from the electric machine directly. In electric vehicles, there are two big categories of traction control methods: slip-based and non-slip-based methods [10].

The implementation of slip-based methods contains three steps: (1) Estimation of the maximum friction coefficient and the corresponding slip ratio; (2) estimation of the real-time driven wheel slip ratios and (3) control of traction torque applied on driven wheels to ensure slip ratio within a correct range [1]. Many difficulties present when conducting these three steps. Firstly, various road/tire conditions cause many uncertainties regarding the slip ratio to achieve the maximum friction coefficient [14]. The tire non-linear characteristics make the performance of some friction coefficient estimators even worse [15, 16]. Secondly, slip estimation is complicated in all-wheel-driven vehicles, when there is no non-driven wheel directly used for calculating vehicle speeds. One solution is to use high-accuracy Global Positioning System sensors, but their costs are relatively high [17]. Other solutions, such as using vehicle kinematic models [18] or vehicle dynamic models [19, 20], can also estimate vehicle speeds. But their estimation accuracies may be reduced due to vehicle parameter variations. Thirdly, precise control of traction torque is important and also not easy to achieve. For example, proportional integral derivative (PID) control is widely used due to its convenient implementation, but its parameters are only tuned under a limited number of cases, making the control system stability relatively low [21, 22]. According to Ref. [23], model predictive control (MPC) shows better traction performance than PID control due to the implementation of the non-linear model. However, MPC needs much more computing resources, which makes its practical application harder [24]. In addition, fuzzy logic is also utilised in some studies to maintain slip ratios by controlling traction torque. Optimisation methods (such as: Genetic Algorithms) can effectively calculate controller parameters [25, 26]. However, if empirical functions are used in the controllers, the fuzzy logic performance will depend on these functions' accuracies [27, 28].

The TSCs based on non-slip-based methods, on the contrary, do not need the driven wheel slip ratio information to control the traction torque. For example, the model following control (MFC) calculates errors between the measured and estimated wheel linear speeds. Torque reduction will be applied when this error is too big [29]. However, the MFC is sensitive to the variation of the vehicle model parameters. Maximum transmissible torque estimation (MTTE) is another non-slip-based TSC method, which estimated the maximum traction torque based on the driven wheel rotational variables and electric machine reference torques [30]. But different road/tire conditions can limit the MTTE performance [31].

Based on the above discussion, different difficulties exist in different TCS methods. Moreover, some methods are over-complex and require much calculation. Considering these challenges, an open-loop slip ratio control method is proposed. This method uses the information of the driven wheel rotational acceleration to detect the wheel spin. By having two steps of reduction on the electric machine reference torque, the driven wheel slip ratio is stably maintained. This method avoids the complexities of doing vehicle speed and slip ratio estimation, thus saving a lot of computation resources of vehicle control units. In addition, by implementing this method in the decentralised drivetrain systems, it is easy to realise the localised control of one driven wheel connected to one electric machine. The rest of the paper is arranged as below: Section 2 describes the vehicle models and analyses the slip ratio behaviours; Section 3 presents the proposed acceleration-based wheel slip control (AWSC) method; Section 4 verifies the proposed method by showing some simulation results; and in Section 5 some conclusions are finally given.

2 | VEHICLE MODELLING

A medium-size vehicle is selected as the reference vehicle in this work. A decentralised electric drivetrain system is used, which has two electric machines providing torque/power to the rear-left and the real-right wheels independently. There are two stages of rotational speed reduction between each electric machine rotor and wheel. Some key parameters of the reference vehicle are listed in Table 1.

The modelling of the reference vehicle is implemented with CarMaker, which is a commercial virtual vehicle testing platform. Vehicle dynamics in longitudinal, lateral, and vertical directions are all considered in the vehicle model. However, since TCSs focus more on the longitudinal vehicle movement, only longitudinal vehicle dynamics are introduced in this section. A free body diagram (FBD) of the vehicle is shown in Figure 1. The vehicle longitudinal acceleration (a) is calculated as:

$$m \cdot a = F_t - F_r \tag{1}$$

where m is the vehicle mass; F_t is the traction force; and F_r is the resistance force, which is the sum of three parts: aerodynamic drag force (F_{aero}), rolling resistance force (F_{roll}), and gradient force (F_{grad}). They are calculated as below:

TABLE 1 Parameters of the reference vehicle

Parameters	Value	Unit
Vehicle mass	1475	kg
Vehicle frontal area	2.34	m^2
Vehicle aerodynamic drag coefficient	0.24	-
Vehicle rolling resistance coefficient	0.018	-
Wheel rotational inertia	2.673	$Kg \cdot m^2$
Wheel radius	0.343	m
First stage gear reduction ratio	3	-
Second stage gear reduction ratio	4	-

$$F_{\text{aero}} = \frac{1}{2} \cdot \rho \cdot A \cdot C_d \cdot v^2 \tag{2}$$

$$F_{\text{roll}} = m \cdot g \cdot C_r \tag{3}$$

$$F_{\text{grad}} = m \cdot g \cdot \sin\theta \tag{4}$$

where ρ is the air density; A is the vehicle frontal area; C_d is the aerodynamic drag coefficient; v is the longitudinal vehicle speed; g is the gravity acceleration; C_r is the rolling resistance coefficient; and θ is the road slope angle.

Free body diagrams of the non-driven front wheel and the driven rear wheel are shown in Figure 2. The dynamic equations of the wheels can be described as:

$$J_f \cdot \dot{\omega}_f = F_{\text{xf}} \cdot r - F_{\text{zf}} \cdot e_f \tag{5}$$

$$J'_r \cdot \dot{\omega}_r = T_w - F_{\text{zr}} \cdot e_r - F_t \cdot r \tag{6}$$

where r is the wheel radius. F_{zf} and F_{zr} are the vertical forces applied on the front and the rear wheels, respectively. The vertical force is determined by vehicle centre of gravity (COG) position, longitudinal acceleration etc. e is the misalignment between the vertical force and the centre of the wheel in the longitudinal direction. This misalignment is caused by the uneven vertical force distribution on tire/road contacting surfaces and is also the reason for the rolling resistance calculated in Ref. (3). F_{xf} is the longitudinal force applied to the front non-driven wheel. T_w is the driving torque applied on the rear dri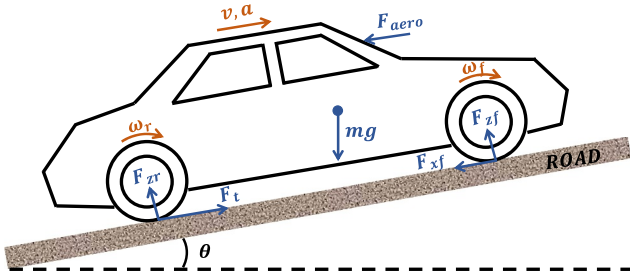ven wheel, which is transmitted from the electric machine after two stages of gears. $\dot{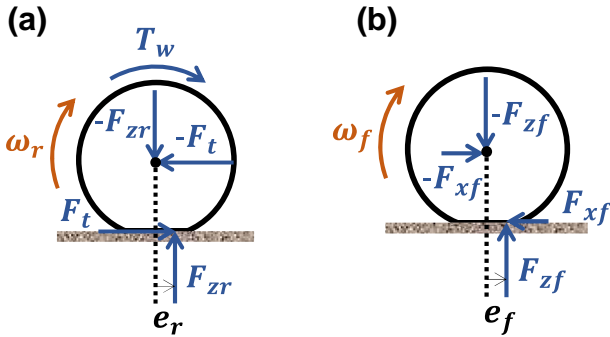\omega}_f$ and $\dot{\omega}_r$ are the front and the rear wheel rotational acceleration, respectively. J_f is the front wheel rotational inertia. J'_r is the rear wheel equivalent rotational inertia, which can be calculated as given below:

$$J'_r = J_r + J_e \cdot (i_1 \cdot i_2)^2 \tag{7}$$

where J_r is the rear wheel rotational inertia; J_e is the rotational inertia of the electric machine rotor; and i_1 and i_2 are the first and the second stage gear reduction ratios. Here, the rotational inertia of the transmission is ignored.

According to Ref. (1), a higher traction force makes the acceleration also bigger. Here, the traction force is calculated from the famous 'Magic Formula' as shown below [32]:

$$F_t = D \cdot \sin\left(C \cdot \tan^{-1}\left(B \cdot \lambda - E \cdot \left(B \cdot \lambda - \tan^{-1}(B \cdot \lambda)\right)\right)\right) \tag{8}$$

where λ is the wheel slip ratio, which describes the difference between the driven wheel linear speed and the vehicle speed:

$$\lambda = \frac{r \cdot \omega_r - v}{|r \cdot \omega_r|} \tag{9}$$

where ω_r is the rear driven wheel rotational speed. The other parameters B, C, D and E in Ref. (8) are determined by tire stiffness, road/tire contacting surface condition, and vertical force applied on the driven wheel.

Figure 3 is an example of Ref. (8). When the slip ratio is small, the traction force is in almost direct proportion to the slip ratio. This relationship can be described with a factor k:

$$F_t = k \cdot \lambda \tag{10}$$

Combining Ref. (1)-(4) and Ref. (10), the slip ratio can be expressed as:

$$\lambda = \frac{1}{k} \cdot \left(m \cdot a + \frac{1}{2}\rho \cdot A \cdot C_d \cdot v^2 + m \cdot g \cdot C_r + m \cdot g \cdot \sin\theta\right) \tag{11}$$

FIGURE 1 Free body diagram of the vehicle.

FIGURE 2 Free body diagrams of the wheels (a) Rear driven wheel and (b) Front non-driven wheel
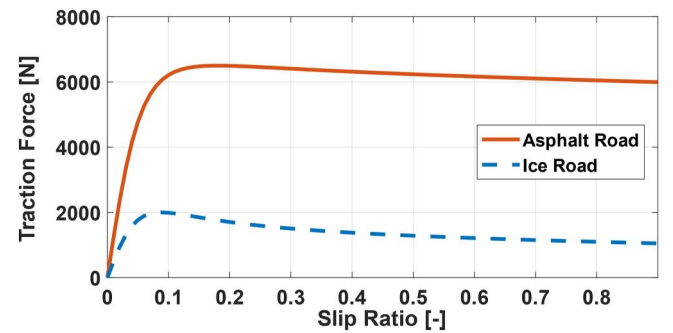

FIGURE 3 The relationship between the traction force and slip ratio calculated from the Magic Formula for two different road surfaces

The slip behaviour under different driving conditions can be analysed by calculating the derivative of Ref. (11):

$$\dot{\lambda} = \frac{1}{k} \cdot (m \cdot \dot{a} + \rho \cdot A \cdot C_d \cdot v \cdot a) \qquad (12)$$

The first condition is when the vehicle is cruising at a constant speed. The derivatives of longitudinal acceleration and speed are both zero. The derivative of the slip ratio also results in zero. This means that the slip ratio is constant when the vehicle speed is unchanged. The second condition is when the vehicle is driven with a constant acceleration when $\dot{a}$ is kept at zero. However, the second item of the right hand side of Ref. (12) increases linearly with time. As a result, there is a linear increase in the slip ratio. This can also be explained as follows: a bigger slip is needed to create the bigger traction force to overcome the increased aerodynamic force. If the aerodynamic force is ignored under low vehicle speed, the slip ratio remains unchanged under constant vehicle acceleration.

As explained, the parameters in Ref. (8) are related to road/tire conditions. Actually, the factor k is largely reduced when the vehicle is driven from an asphalt road to an ice road. So, Ref. (11) and Ref. (12) cannot be used to analyse slip ratio change under this case. Instead, the derivative of Ref. (9) can be utilised.

$$\dot{\lambda} = \frac{v \cdot \dot{\omega}_r}{r \cdot \omega_r{}^2} - \frac{a}{r \cdot \omega_r} \qquad (13)$$

When the vehicle arrives on an ice road, the traction force will reduce suddenly, which can also be observed from Figure 3. According to Ref. (6), the driven wheel rotational acceleration will increase if T_w is kept unchanged. On the contrary, the vehicle longitudinal acceleration will decrease according to Ref. (1). As a result, the wheel slip derivative in Ref. (13) starts to increase. When F_t reaches its maximum value with the increasing slip ratio and if $(F_t \cdot r)$ is still smaller than T_w, the driven wheel will spin. Similarly, when the vehicle is started from an ice road with T_w higher than the maximum $(F_t \cdot r)$, the driven wheel will also keep having high slip ratios and spin. The spinning of the driven wheel makes the traction force drop, which can be seen in Figure 3 when the slip ratio is bigger than 0.2 on an asphalt road and 0.1 on an ice road. The proposed slip control method will be introduced in the next section to solve this problem.

3 | ACCELERATION-BASED WHEEL SLIP CONTROL (AWSC)

The flow chart of the proposed acceleration-based wheel slip control (AWSC) is shown in Figure 4. As explained, when the vehicle is driven from an asphalt road to an ice road, the rotational acceleration of the driven wheel will increase due to the loss of traction force. This rotational acceleration is obviously greater than that of normal driving, considering the vehicle's maximum acceleration performance. So, the driven wheel rotational acceleration is continuously compared with a
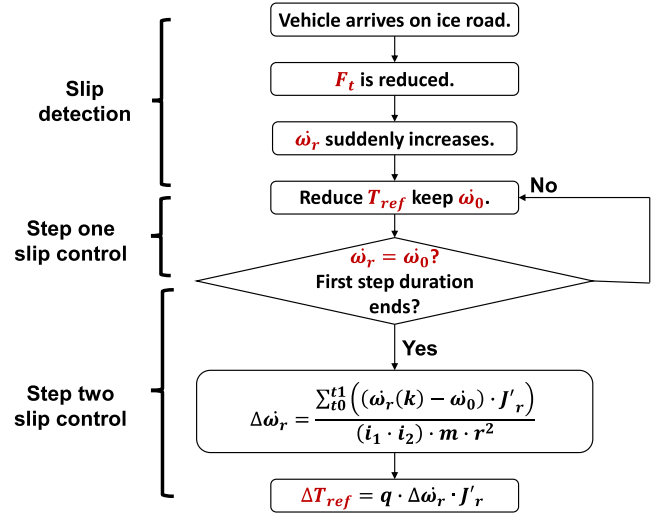

FIGURE 4 Flow chart of the acceleration-based wheel slip control

threshold value to determine the wheel spin that is happening. The slip control is done by two steps in this method. The first step is to reduce the driven wheel rotational acceleration back to the value before the driven wheel starts to spin. This requires that the driven wheel rotational acceleration is recorded and updated. The one before spin being detected is used as the reference rotational acceleration ($\dot{\omega}_0$) for the first step. Then, the reference torque for controlling the electric machine is set as follows:

$$T_{\text{ref}}(k+1) = T_{\text{ref}}(k) - \frac{\left(\dot{\omega}_r(k) - \dot{\omega}_0\right) \cdot J'_r}{i_1 \cdot i_2} \qquad (14)$$

where $T_{\text{ref}}(k)$ and $T_{\text{ref}}(k+1)$ are the electric machine reference torques at the time-step k and $k+1$, respectively; $\dot{\omega}_r(k)$ is the driven wheel rotational acceleration at the time step k. The traction force reduction caused by the ice road is gradual as the change in the deformation of the tire needs time. Therefore, the reference torque adjustment according to Ref. (14) is done for many time-steps. At the end of the first step, the traction torque is not further reduced, and the driven wheel rotational acceleration is also kept around $\dot{\omega}_0$.

After the first step of torque reduction, the first item in the right hand side of Ref. (13) remains unchanged. However, the second item is reduced due to the loss of traction force, which can be calculated from Ref. (1). As a result, the derivative of the slip ratio is bigger than zero after the first step. This means the first step of reference torque reduction is not enough to prevent wheel slip from increasing. Therefore, the second step of torque reduction is needed. The relationship between the electromagnetic torque of the electric machine and the traction force can be expressed as below:

$$T_{\text{em}}(k) \cdot (i_1 \cdot i_2) = F_t(k) \cdot r + J'_r \cdot \dot{\omega}_r(k) + F_{zr} \cdot e_r \qquad (15)$$

In the first step, since the reference torque is adjusted to maintain the driven wheel rotation acceleration at $\dot{\omega}_0$, the

relationship between the electric machine reference torque and the traction force is:

$$T_{\mathrm{ref}}(k) \cdot (i_1 \cdot i_2) = F_t(k-1) \cdot r + J'_r \cdot \dot{\omega}_0 + F_{\mathrm{zr}}(k) \cdot e_r \quad (16)$$

The $(k-1)$ in Ref. (16) is because the previous time-step variables are used to calculate the reference torque in the current time-step. By considering the high bandwidth of the electric machine torque control, the electric machine torque in Ref. (15) and the reference torque in Ref. (16) can be assumed to be the same. These two equations can be combined to get the following one:

$$(F_t(k) - F_t(k-1)) \cdot r = (\dot{\omega}_r(k) - \dot{\omega}_0) \cdot J'_r \quad (17)$$

By integrating Ref. (17), the traction force reduction during the first step can be calculated as given below:

$$\Delta F_t = \frac{1}{r} \cdot \sum_{t_0}^{t_1} \left((\dot{\omega}_r(k) - \dot{\omega}_0) \cdot J'_r \right) \quad (18)$$

where t_0 and t_1 are the starting and the end times of the first step, respectively. The vehicle acceleration change by the traction force reduction is:

$$\Delta a = \frac{\Delta F_t}{m} \quad (19)$$

In order to cancel the driven wheel slip ratio change caused by this vehicle acceleration reduction, the driven wheel rotational acceleration shall be reduced as well to make the slip ratio derivative in Ref. (13) zero, which is calculated as below:

$$\Delta \dot{\omega}_r = \frac{\Delta a}{r} \quad (20)$$

To have this rotational acceleration reduction, the electric machine reference torque should be reduced further, which is the second step of the slip ratio control. This reference torque reduction is calculated as:

$$\Delta T_{\mathrm{ref}} = \frac{\Delta \dot{\omega}_r \cdot J'_r}{i_1 \cdot i_2} \quad (21)$$

The block diagram of the proposed AWSC is shown in Figure 5a, and details of the electric machine block are described in Figure 5b. There are two inputs to the electric machine block: electric machine speed (ω_{em}) and electric machine reference torque (T_{ref}). These two inputs are used to find out reference d- and q-axis currents in a look-up table, which is obtained according to the maximum torque per ampere (MTPA) control strategy. Two proportional integral (PI) controllers are used to give d- and q-axis voltages, which are then used to calculate actual d- and q-axis currents from the electric machine model. Considering the number of pole pair (n_p),

magnet flux linkage (Ψ_m), d-axis inductance (L_d), and q-axis inductance (L_q), the electric machine electromagnetic torque (T_{em}) is calculated, which is also the only output torque of the electric machine block. The rest of the AWSC block diagram follows the proposed slip ratio control strategy by having two-step torque reduction. As is explained, the first step is to maintain the driven wheel acceleration at the reference value. The performance of this step is mainly affected by the rotational speed sensor accuracy and current control bandwidth of the electric machine. The second step is to reduce the slip ratio derivative back to zero. The performance of this step is affected by some vehicle parameter estimation. For example, the influence of the vehicle mass is shown as given below:

$$\Delta T_{\mathrm{ref}} = \frac{\sum_{t_0}^{t_1} \left((\dot{\omega}_r(k) - \dot{\omega}_0) \cdot J'_r \right)}{(i_1 \cdot i_2) \cdot (m + \Delta m) \cdot r^2} \cdot J'_r \quad (22)$$

where Δm is the perturbation of the vehicle mass caused by change of the passengers, cargo, fuel etc. Obviously, when the Δm is bigger than zero, the reference torque reduction in the second step will be smaller. As a result, the slip ratio will keep increasing. On the contrary, if the Δm is smaller than zero, the slip is well controlled. However, the reference torque is over reduced, and the vehicle acceleration is also smaller. Normally, the controllability and safety of the vehicle are more important than its acceleration performance. Hence, a factor q is given to the calculated reference torque reduction value in the second step. This factor shall be selected as a value bigger than one, and the final expression of the ΔT_{ref} is shown as below:

$$\Delta T_{\mathrm{ref}} = q \cdot \frac{\sum_{t_0}^{t_1} \left((\dot{\omega}_r(k) - \dot{\omega}_0) \cdot J'_r \right)}{(i_1 \cdot i_2) \cdot m \cdot r^2} \cdot J'_r \quad (23)$$

4 | SIMULATION VERIFICATION

4.1 | Simulation platform

The proposed control strategy is verified by simulations. The simulation platform consists of a high-fidelity vehicle model in CarMaker and an electric drive model in PLECS. Both models are implemented in the Simulink environment and combined as shown in Figure 6. The vehicle model consists of the modelling of the driver, autobody, tire, road, environment, and driving mission. The driver model gives the information of gas (θ_g) and brake (θ_b) pedal positions, so that the vehicle can follow the driving mission. The vehicle controller converts the gas pedal position information into the driver-demanded electric machine torque (T_{driver}). The driven wheel rotational speed can also be obtained from the vehicle model. There are two outputs to the electric drive model. The only input of the vehicle model is the electromagnetic torque of the electric machine. The vehicle linear speed calculated from the autobody and wheel model is sent to the driver model, realising the
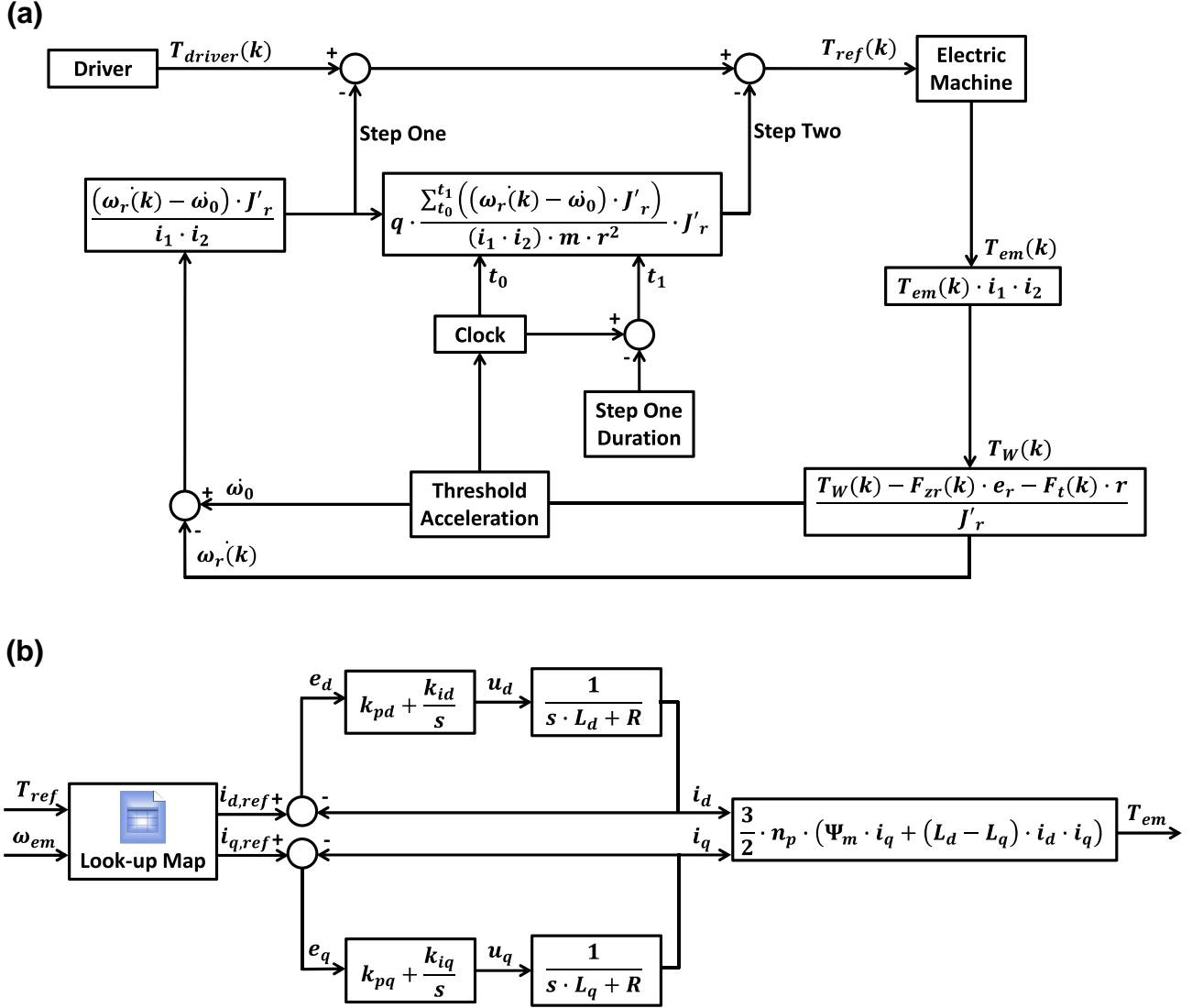
(a)

(b)

FIGURE 5   (a) Block diagram of the acceleration-based wheel slip control and (b) Electric machine block details

vehicle speed close-loop control. The road and environment model provides information on road friction coefficient, road gradient, air density, wind speed etc.

The electric drive model in PLECS consists of the modelling of the electric machine, inverter, DC supply and controller. The AWSC method is also implemented inside the electric drive model and adjusts the driver-demanded torque to electric machine reference torque. The electric machine rotational speed is calculated from the driven wheel speed according to:

$$\omega_{em} = \omega_r \cdot i_1 \cdot i_2 \qquad (24)$$

The reference torque and electric machine speed are used to calculate the reference currents for the field-oriented-control (FOC) of the electric machine. Based on controlled currents, electromagnetic torque can be calculated, which is fed back to the vehicle model.
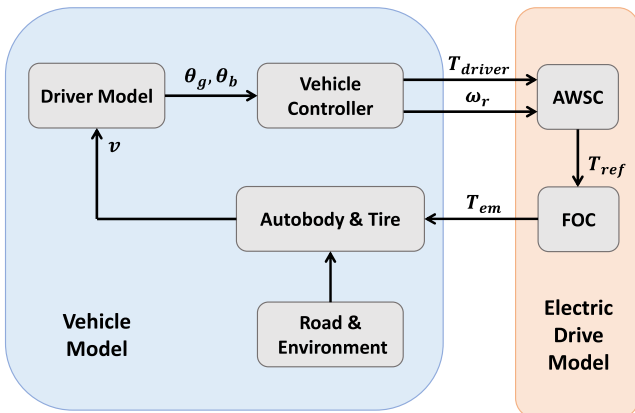
4.2 | Simulation results

During the simulation, the vehicle is accelerated by applying a constant gas pedal position. The vehicle is started on an asphalt road. Then it enters an ice road after 25 m. Simulation results are shown in Figure 7 to Figure 9. The simulation results of the first 10 seconds are presented in the figure 7a, and zoom-in figures before the AWSC is activated are presented in the figure 7b. Figure 7 shows the distance travelled, linear speed, and linear acceleration of the vehicle. Figure 8 presents the slip detection and torque reduction details. The first subplot shows trigger signals of the first and the second step of the slip control. The torque reduction in two steps is shown in the second subplot. The third subplot shows the driver-demanded electric machine torque, the electromagnetic torque from the machine, and the load torque applied on the machine shaft. Figure 9 shows the driven wheel rotational speed and rotational acceleration. The wheel slip ratio and the reference value

of the wheel rotational acceleration used in the first step of control are also shown.

As can be observed in Figure 8, the electromagnetic torque increases gradually at the beginning. This is because it takes some time before the gas pedal is actuated to the target position and for the traction force to be built up. Otherwise, sufficient traction force cannot be built up to follow the driving torque, and the vehicle will not be able to start normally. It can also be seen from the gradual increasing of the driver-demanded torque. The slip ratio in Figure 9 is high when the vehicle is started from the standstill. This is because the vehicle linear speed is close to zero at the beginning. As the vehicle speed increases, the slip ratio will gradually drop to the normal range. The linear acceleration in Figure 7 follows the load torque. Consequently, the slope of the vehicle speed curve increases and becomes constant after approximately 2 seconds.

When the vehicle enters ice at 4.2 s, the traction force applied from the road to the tire will drop immediately due to the low friction coefficient, which can be observed by the drop of the load torque in Figure 8. However, the driving torque applied on the wheel remains the same. According to Ref. (6), the driven wheel will accelerate much faster, which can be observed by the sudden jump in the wheel acceleration, as can be seen in Figure 9. As mentioned before, the driven wheel rotational acceleration is used to detect the spin that is happening. Therefore, the step one trigger signal in Figure 8 goes from low to high. After the trigger, the step one torque reduction is applied, and the value for each time-step is calculated according to Ref. (14). Due to this, the rotational acceleration of the wheel drops in the following time-step. However, the rotational acceleration increases in the next time-step. This is because the difference between the driving torque and the load torque becomes bigger. This bigger difference is from the even bigger load torque drop. Therefore, the wheel acceleration increases and reaches the maximum. As more torque reduction is applied, the mentioned difference becomes smaller, causing the wheel acceleration to reduce and reach the reference value. Afterwards, the wheel acceleration oscillates around the reference value.

After the end of the first step duration, the trigger signal of the second step is turned on. The torque reduction calculated from the integration is applied, which causes the wheel acceleration to be negative. This is because the load torque is now slightly higher than the driving torque. It means the driving torque is reduced more than necessary. It is due to the selection of the factor q in Ref. (23), as safety is prioritised over performance. Afterwards, the load torque reduces gradually and becomes smaller than the driving torque. The wheel rotational acceleration also becomes positive, but smaller than the reference value in step one. The wheel slip ratio increases when the vehicle enters the ice due to the increased wheel speed. It drops when the second step torque reduction is

FIGURE 6 Dataflow between the vehicle model in CarMaker and the electric drive model in PLECS
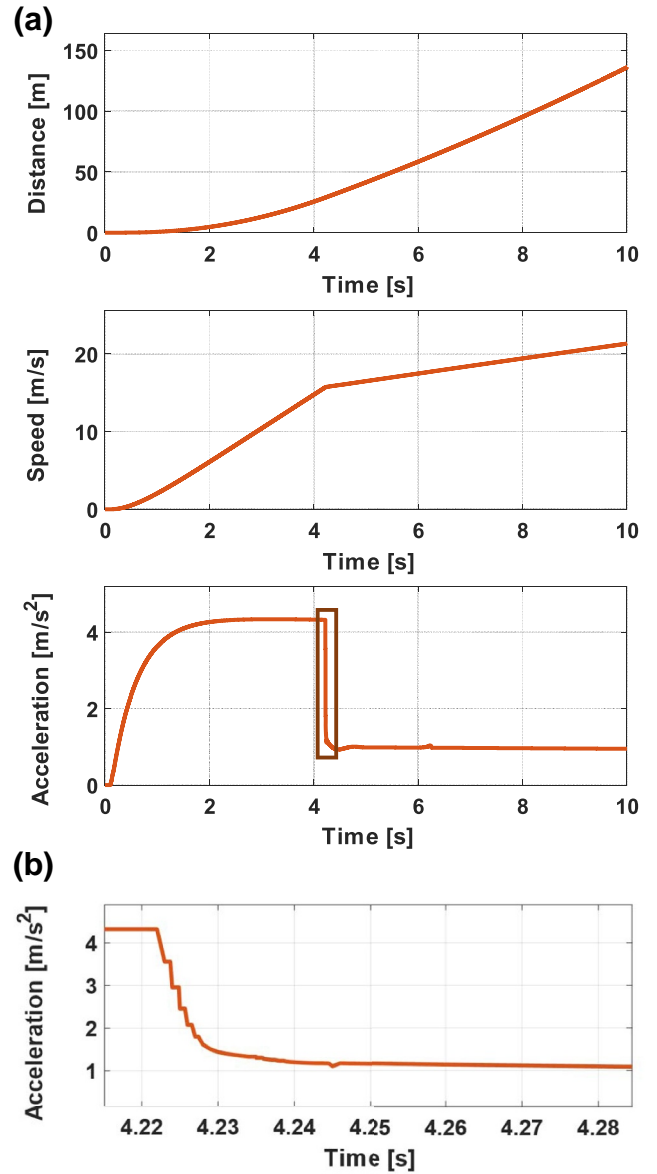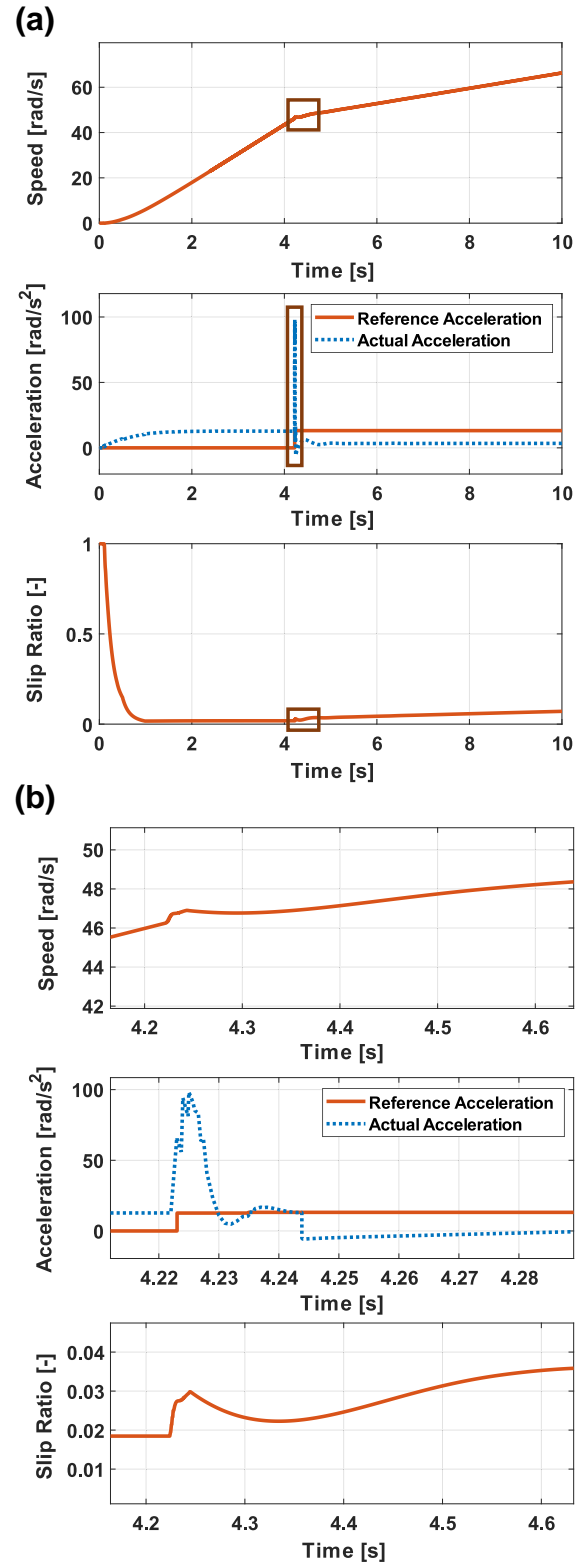

FIGURE 7 Simulation results showing travelled distance, linear speed and acceleration of the vehicle, when driving with a constant gas pedal position from an asphalt road to an ice road. (a) First ten-second simulation results; (b) Zoom-in figures just before acceleration-based wheel slip control (AWSC) is activated
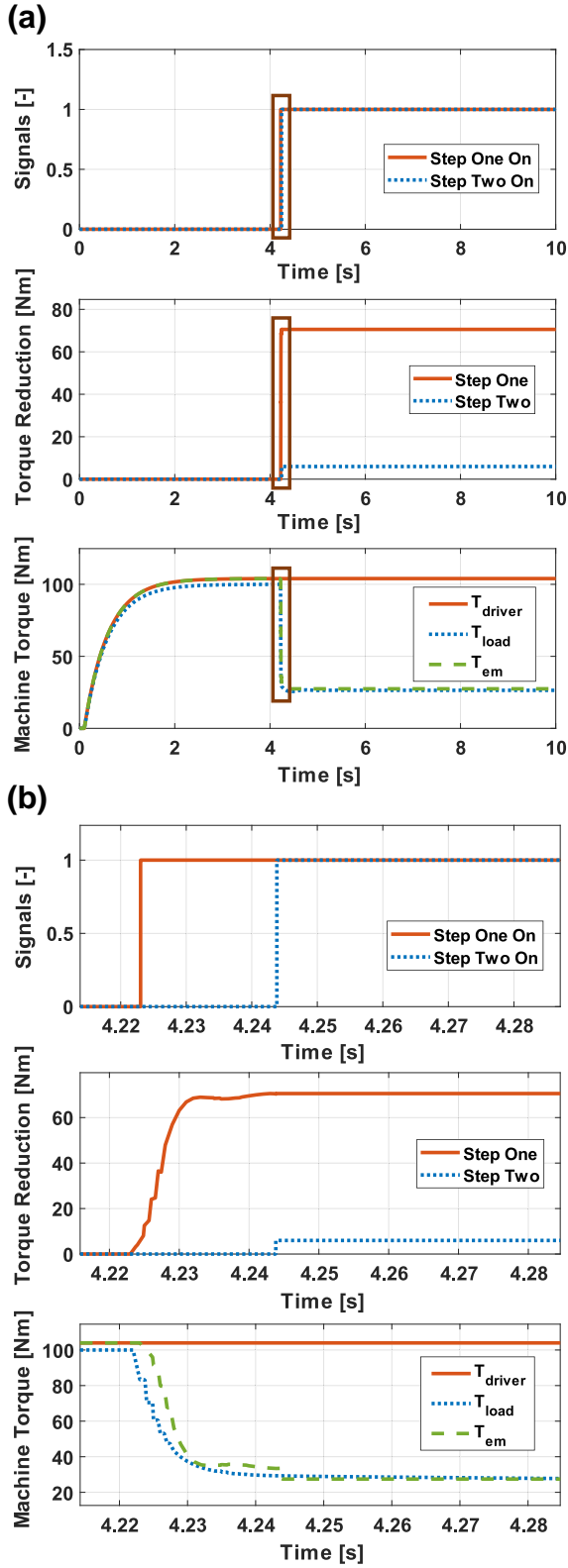
FIGURE 8 Simulation results showing acceleration-based wheel slip control (AWSC) control signals and effects on electric machine torque, when driving with a constant gas pedal position from an asphalt road to an ice road. (a) First ten-second simulation results; (b) Zoom-in figures just before AWSC is activated

FIGURE 9 Simulation results of the driven wheel rotational speed, rotational acceleration, and slip ratio when driving with a constant gas pedal position from an asphalt road to an ice road. (a) First ten-second simulation results; (b) Zoom-in figures just before acceleration-based wheel slip control (AWSC) is activated

applied as the wheel stops accelerating. Afterwards, the slip ratio increases to the normal range and keeps almost constant when the vehicle is accelerated on the ice road.

5 | CONCLUSIONS

An acceleration-based wheel slip control for regulating driving torque on the driven wheel is proposed. The longitudinal dynamics of the vehicle are analysed to understand slip ratio behaviours under different driving scenarios. When the vehicle travels over to a low friction road, the rapid change in the driven wheel rotational acceleration caused by the traction force reduction is used to detect wheel spin. The driving torque on the wheel is reduced in two steps. In the first step, the wheel acceleration is controlled back to the reference, which is determined as the value before the wheel starts to spin. In the second step, the traction force reduction is estimated and used for further reduction of wheel acceleration, avoiding the increase in slip ratio.

An electric vehicle with a decentralised electric drivetrain system is modelled. The vehicle has two independent rear-driven wheels. The vehicle model is realised using a vehicle simulation platform, CarMaker. The electric drive system is modelled in an electrical simulation tool, PLECS. Both models are implemented in the Simulink environment to verify the proposed control method. In the simulation, the vehicle travels on an asphalt road and then an ice road with the same acceleration request. Simulation results show the proposed method works well to meet the expected anti-slip functionalities. The control is fast enough to react on the sudden change of wheel acceleration without significant wheel spin being observed. The high bandwidth control of electric machines allows the fast regulation of the driving torque, and wheel acceleration can be controlled back to the normal range within half a second.

CONFLICTS OF INTEREST
The authors declare that there is no conflict of interest.

DATA AVAILABILITY STATEMENT
Data sharing not applicable to this article as no datasets were generated or analysed during the current study.

NOMENCLATURE

g	Gravity acceleration [m/s^2]
ρ	Air density [kg/m^3]
θ	Road slope angle [rad]
m	Vehicle mass [kg]
Δm	Vehicle mass perturbation [kg]
A	Vehicle frontal area [m^2]
C_d	Vehicle aerodynamic drag coefficient [-]
C_r	Vehicle rolling resistance coefficient [-]
r	Wheel radius [m]
J_f	Front wheel rotational inertia [kg $\cdot$ m^2]
J'_r	Rear wheel equivalent rotational inertia [kg $\cdot$ m^2]
J_r	Rear wheel rotational inertia [kg $\cdot$ m^2]
J_e	Electric machine rotor rotational inertia [kg $\cdot$ m^2]
i_1	First stage gear reduction ratio [-]
i_2	Second stage gear reduction ratio [-]
e_f	Front wheel vertical force misalignment [m]
e_r	Rear wheel vertical force misalignment [m]
a	Vehicle longitudinal acceleration [m/s^2]
v	Vehicle longitudinal speed [m/s]
ω_f	Front wheel rotational speed [rad/s]
ω_r	Rear wheel rotational speed [rad/s]
ω_{em}	Electric machine rotational speed [rad/s]
$\dot{\omega}_f$	Front wheel rotational acceleration [rad/s^2]
$\dot{\omega}_r$	Rear wheel rotational acceleration [rad/s^2]
$\dot{\omega}_0$	Wheel reference rotational acceleration [rad/s^2]
λ	Wheel slip ratio [-]
$\dot{\lambda}$	Derivative of wheel slip ratio [-]
F_t	Vehicle traction force [N]
F_r	Vehicle resistance force [N]
F_{aero}	Vehicle aerodynamic drag force [N]
F_{roll}	Vehicle rolling resistance force [N]
F_{grad}	Vehicle gradient force [N]
F_{xf}	Front wheel longitudinal force [N]
F_{zf}	Front wheel vertical force [N]
F_{zr}	Rear wheel vertical force [N]
T_w	Rear wheel driving torque [N $\cdot$ m]
T_{driver}	Driver demanded electric machine torque [N $\cdot$ m]
T_{ref}	Electric machine reference torque [N $\cdot$ m]
T_{em}	Electric machine electromagnetic torque [N $\cdot$ m]
ΔF_t	First step traction force reduction [N]
ΔT_{ref}	Second step reference torque reduction [N $\cdot$ m]

ORCID
Bowen Jiang https://orcid.org/0000-0003-1425-6771

REFERENCES
1. Leng, B., et al.: Robust variable structure anti-slip control method of a distributed drive electric vehicle. IEEE Access. 8, 162196–162208 (2020). https://doi.org/10.1109/ACCESS.2020.3021694
2. Jiang, B., et al.: Real-time FPGA/CPU-based simulation of a full-electric vehicle integrated with a high-fidelity electric drive model. Energies. 15(5) 1824 (2022). https://doi.org/10.3390/en15051824
3. Zhai, L., et al.: Continuous steering stability control based on an energy-saving torque distribution algorithm for a four in-wheel-motor independent-drive electric vehicle. Energies. 11(2)350 (2018). https://doi.org/10.3390/en11020350
4. Huang, J., et al.: Multi-Objective optimization control of distributed electric drive vehicles based on optimal torque distribution. IEEE Access. 7, 16377–16394 (2019). https://doi.org/10.1109/ACCESS.2019.2894259
5. Hu, J., et al.: An optimal torque distribution control strategy for four-wheel independent drive electric vehicles considering energy economy.

IEEE Access. 7, 141826–141837 (2019). https://doi.org/10.1109/ACCESS.2019.2944479

6. Ding, X., Wang, Z., Zhang, L.: Event-triggered vehicle sideslip angle estimation based on low-cost sensors. IEEE Trans. Ind. Inf. 18(7), 4466–4476 (2022). https://doi.org/10.1109/TII.2021.3118683

7. Ding, X., Wang, Z., Zhang, L.: Hybrid control-based acceleration slip regulation for four-wheel-independent-actuated electric vehicles. IEEE Trans Elec. 7(3), 1976–1989 (2021). Sept. 2021. https://doi.org/10.1109/TTE.2020.3048405

8. Subramaniyam, K.V., Subramanian, S.C.: Electrified vehicle wheel slip control using responsiveness of regenerative braking. IEEE Trans. Veh. Technol. 70(4), 3208–3217 (2021). https://doi.org/10.1109/TVT.2021.3066095

9. Reichensdörfer, E., Odenthal, D., Wollherr, D.: On the stability of nonlinear wheel-slip zero dynamics in traction control systems. IEEE Trans. Control Syst. Technol. 28(2), 489–504 (2020). https://doi.org/10.1109/TCST.2018.2880932

10. Ivanov, V., Savitski, D., Shyrokau, B.: A survey of traction control and antilock braking systems of full electric vehicles with individually controlled electric motors. IEEE Trans. Veh. Technol. 64(9), 3878–3896 (2015). https://doi.org/10.1109/TVT.2014.2361860

11. Montani, M., et al.: Performance review of three car integrated ABS types: development of a tire independent wheel speed control. Energies. 13(23)6183 (2020). https://doi.org/10.3390/en13236183

12. Nadeau, J., Micheau, P., Boisvert, M.: Ideal regenerative braking torque in collaboration with hydraulic brake system. Twelfth International Conference on Ecological Vehicles and Renewable Energies, pp. 1–5. EVER (2017). https://doi.org/10.1109/EVER.2017.7935934

13. Qian, W., et al.: Using high-control-bandwidth FPGA and SiC inverters to enhance high-frequency injection sensorless control in interior permanent magnet synchronous machine. IEEE Access. 6, 42454–42466 (2018). https://doi.org/10.1109/ACCESS.2018.2858199

14. Cheng, S., et al.: Adaptive unified monitoring system design for tire-road information. ASME. J. Dyn. Sys., Meas., Control. 141(7), 071006 (2019). https://doi.org/10.1115/1.4043113

15. Chen, J., et al.: UKF-based adaptive variable structure observer for vehicle sideslip with dynamic correction. IET Control Theory & Appl. 10(14), 1641–1652 (2016). https://doi.org/10.1049/iet-cta.2015.1030

16. Zhao, J., Zhang, J., Zhu, B.: Coordinative traction control of vehicles based on identification of the tyre–road friction coefficient. Proc. Inst. Mech. Eng. D, J. Automobile Eng. 230(12), 1585–1604 (2016). https://doi.org/10.1177/0954407015618041

17. Ding, X., et al.: Longitudinal vehicle speed estimation for four-wheel-independently-actuated electric vehicles based on multi-sensor fusion. IEEE Trans. Veh. Technol. 69(11), 12797–12806 (2020). Nov. 2020. https://doi.org/10.1109/TVT.2020.3026106

18. Zhang, Y., et al.: Distributed Drive Electric Vehicle Longitudinal Velocity Estimation with Adaptive Kalman Filter: Theory and Experiment SAE Technical Paper 2019-01-0439 https://doi.org/10.4271/2019-01-0439 (2019)

19. Zhao, Z.-G., et al.: Distributed and self-adaptive vehicle speed estimation in the composite braking case for four-wheel drive hybrid electric car. Veh. Syst. Dyn. 55(5), 750–773 (2017). https://doi.org/10.1080/00423114.2017.1279739

20. Heidfeld, H., Schünemann, M., Kasper, R.: Experimental validation of a GPS-aided model-based UKF vehicle state estimator. In: IEEE International Conference on Mechatronics (ICM), pp. 537–543 (2019). https://doi.org/10.1109/ICMECH.2019.8722942

21. Wu, L., et al.: Acceleration slip regulation strategy for distributed drive electric vehicles with independent front axle drive motors. Energies. 8(5), 4043–4072 (2015). https://doi.org/10.3390/en8054043

22. Savitski, D., et al.: Improvement of traction performance and off-road mobility for a vehicle with four individual electric motors: driving over icy road. J. Terramechanics. 69, 33–43 (2017). https://doi.org/10.1016/j.jterra.2016.10.005

23. Tavernini, D., et al.: Explicit nonlinear model predictive control for electric vehicle traction control. IEEE Trans. Control Syst. Technol. 27(4), 1438–1451 (2019). https://doi.org/10.1109/TCST.2018.2837097

24. Sekour, M., Hartani, K., Merah, A.: Electric vehicle longitudinal stability control based on a new multimachine nonlinear model predictive direct torque control. J. Adv. Transport., 1 (2017). https://doi.org/10.1155/2017/4125384

25. Fabrício Leonardo Silva, L.C., et al.: Parameter influence analysis in an optimized fuzzy stability control for a four-wheel independent-drive electric vehicle. Control Eng. Pract. 120(2022). ISSN 0967-0661. https://doi.org/10.1016/j.conengprac.2021.105000

26. Leonardo Silva, F, et al.: Robust fuzzy stability control optimization by multi-objective for modular vehicle. Mech. Mach. Theor. 167(2022) (2022). ISSN 0094-114X. https://doi.org/10.1016/j.mechmachtheory

27. Dahmani, H., Pagés, O., El Hajjaji, A.: Traction control system using a fuzzy representation of the vehicle model. In: American Control Conference, pp. 5712–5717. ACC (2015). https://doi.org/10.1109/ACC.2015.7172234

28. Hartani, K., et al.: A robust wheel slip control design with radius dynamics observer for EV. SAE Int. J. Veh. Dyn., Stab., and NVH. 2(2), 135–146 (2018). https://doi.org/10.4271/10-02-02-0009

29. Hori, Y.: Future vehicle driven by electricity and control-research on four-wheel-motored 'UOT electric march II. IEEE Trans. Ind. Electron. 51(5), 954–962 (2004). https://doi.org/10.1109/tie.2004.834944

30. Yin, D, Oh, S., Hori, Y.: A novel traction control for EV based on maximum transmissible torque estimation. IEEE Trans. Ind. Electron. 56(6), 2086–2094 (2009). https://doi.org/10.1109/tie.2009.2016507

31. Hu, J., et al.: Electric vehicle traction control: a new MTTE methodology. IEEE Ind. Appl. Mag. 18(2), 23–31 (2012). March-April 2012. https://doi.org/10.1109/MIAS.2011.2175519

32. Bayle, P., Forissier, J.F., Lafon: A new tyre model for vehicle dynamics simulations. In: Automotive Technology International, pp. 193–198 (1993)